

RESEARCH ARTICLE

10.1002/2015PA002806

Key Points:

- SST-driven atmosphere circulation change contributes to Pliocene coastal warmth
- Weak SST gradients reduce upwelling-favorable wind at midlatitude sites in GCM
- Decoupling of SST and productivity does not rule out a wind change mechanism

Correspondence to:

N. P. Arnold,
nathan.arnold@nasa.gov

Citation:

Arnold, N. P., and E. Tziperman (2015), Reductions in midlatitude upwelling-favorable winds implied by weaker large-scale Pliocene SST gradients, *Paleoceanography*, 30, doi:10.1002/2015PA002806.

Received 19 MAR 2015

Accepted 26 NOV 2015

Accepted article online 3 DEC 2015

Reductions in midlatitude upwelling-favorable winds implied by weaker large-scale Pliocene SST gradients

Nathan P. Arnold¹ and Eli Tziperman^{1,2}

¹Department of Earth and Planetary Sciences, Harvard University, Cambridge, Massachusetts, USA, ²School of Engineering and Applied Science, Harvard University, Cambridge, Massachusetts, USA

Abstract The early-to-mid Pliocene (3–5.3 Ma) is the most recent geologic period of significant global warmth. Proxy records of Pliocene sea surface temperature (SST) indicate significant and still unexplained warm anomalies of 3°C–9°C in midlatitude eastern boundary currents, where present-day cool temperatures are maintained by wind-driven upwelling. Here we quantify the effect of large-scale Pliocene-like SST patterns on the surface wind stress around the California, Humboldt, Canary, and Benguela midlatitude coastal upwelling sites. A high-resolution atmosphere model forced with Pliocene SST simulates changes in surface winds that imply reductions of 10% to 50% in both coastal upwelling, driven by alongshore wind stress, and offshore upwelling driven by wind stress curl. These changes result primarily from a reduced meridional temperature gradient which weakens the subtropical highs, and a reduction in zonal land-sea temperature contrast which weakens geostrophic alongshore winds. These results suggest that Pliocene coastal warm anomalies may result in part from atmospheric circulation changes which reduce upwelling intensity. The coastal wind stress and offshore wind stress curl are shown to respond differently to incremental changes in SST, topography, and land surface anomalies. Significant decreases in simulated cloud fraction within the subtropical highs suggest that a weaker land-sea temperature contrast could be maintained by cloud radiative feedbacks.

1. Introduction

The early-to-mid Pliocene (3–5.3Ma) was the most recent geologic era significantly warmer than present and is considered a potential analogue for the next century of anthropogenic global warming [Chandler *et al.*, 1994; Dowsett *et al.*, 1996, 2009, although see Lunt *et al.*, 2009]. Peak Pliocene atmospheric CO₂ concentrations are estimated to have been 400±50 ppm [Raymo *et al.*, 1996; Pagani *et al.*, 2010; Seki *et al.*, 2010; Martínez-Botí *et al.*, 2015], and a combination of proxy records and modeling studies puts the mid-Pliocene peak global average surface temperature about 3–4°C warmer than present, with greater warming toward the poles [Chandler *et al.*, 1994; Dowsett *et al.*, 2011; Brierley *et al.*, 2009; Dowsett *et al.*, 2012, 2013; Fedorov *et al.*, 2013; O'Brien *et al.*, 2014]. The Greenland and West Antarctic ice sheets were greatly diminished and possibly absent for much of this period [Scherer, 1991; Pollard and DeConto, 2009], and global sea level was up to 25 m higher than today [Dowsett and Cronin, 1990; Raymo *et al.*, 2011; Miller *et al.*, 2012; Woodard *et al.*, 2014; Rovere *et al.*, 2014].

Some of the most interesting features of the early Pliocene are the significant warm anomalies found in ocean upwelling zones around the globe. Multiple proxies for sea surface temperature (SST) indicate anomalies of roughly +3°C in the eastern equatorial Pacific, while west Pacific SSTs were similar to modern values, suggesting that mean conditions in the Pliocene equatorial Pacific resembled a modern El Niño event [Chaisson, 1995; Wara *et al.*, 2005; Ravelo *et al.*, 2006; Lawrence *et al.*, 2006; Groeneveld *et al.*, 2006; Dekens *et al.*, 2008], although a recent study argues that the equatorial zonal gradient was comparable to modern [Zhang *et al.*, 2014]. In addition, all four midlatitude upwelling zones associated with major eastern boundary currents—California, Humboldt, Canary, and Benguela—show anomalies of +3°C to +9°C relative to today [Herbert and Schuffert, 1998; Marlow *et al.*, 2000; Dekens *et al.*, 2007]. In the present era, both midlatitude and equatorial upwelling zones are associated with high biological productivity and relatively cool temperatures, maintained by the raising of cold, nutrient-enriched deep waters by local patterns of wind stress [Mann and Lazier, 2005]. Upwelling sites have tremendous economic and ecological importance, supporting a large fraction of ocean biodiversity and roughly 20% of the world's fish catch [Pauly and Christensen, 1995]. There is thus great interest in understanding how upwelling systems will respond to a warmer world [Bakun, 1990; Snyder *et al.*, 2003].

Although the warm anomalies in coastal upwelling zones are supported by multiple sediment cores and proxy types, there is no consensus on a physical explanation, and they are not reproduced in Pliocene simulations by the latest generation of coupled climate models [Haywood *et al.*, 2012]. One hypothesis suggests that the global thermocline was deeper during the Pliocene [Fedorov *et al.*, 2006]. While wind-driven upwelling could still occur, the upwelled water would be drawn from a warmer source, resulting in warm anomalies at the surface. Several mechanisms which might produce a deeper thermocline have been identified, including an enhanced freshwater flux in high latitudes [Fedorov *et al.*, 2004], increased mixing in the subtropics driven by significantly enhanced hurricane activity [Fedorov *et al.*, 2010], a reduced meridional temperature gradient [Boccaletti *et al.*, 2004], and changes in extratropical cloud cover [Barreiro and Philander, 2008; Burls and Fedorov, 2014].

Another possibility is that the surface winds near upwelling zones were weaker or shifted relative to their modern positions. The warm anomalies are then explained as a reduction in upwelling intensity or a shift in the location of upwelling, rather than a change in source water temperature. Tziperman and Farrell [2009] suggested that changes in the intensity or organization of tropical convection could have excited atmospheric waves that propagate out of the tropics. In doing so, these waves transport zonal momentum equatorward, weaken the easterlies there, and may push the tropics toward a more El Niño-like mean state. The same waves are absorbed in the midlatitudes and may alter surface winds around upwelling zones in a manner analogous to the teleconnections associated with El Niño–Southern Oscillation.

Wind stress could also differ due to the large-scale surface temperature field. The modern upwelling-favorable winds around these sites are associated with the subtropical high-pressure zones that result from a combination of the subsiding branch of the zonal mean Hadley circulation and the seasonal land-sea temperature contrast. This results in a land-sea pressure gradient which drives the alongshore geostrophic winds responsible for upwelling. Marlow *et al.* [2000] proposed that changes in upwelling intensity evident in a sediment core from the Benguela Current could be associated with a gradual increase in the trade winds due to the increase in pole-to-equator temperature gradient between the Pliocene and the present. Changes in subsurface water properties and changes in surface wind stress are not mutually exclusive and may both play a role in controlling the temperatures recorded by planktic organisms.

In this study we use global reconstructions of Pliocene SST to estimate the surface winds around midlatitude coastal sites, and by extension, the level of upwelling these winds has the potential to support. We use a high-resolution global atmosphere model driven by two different Pliocene SST reconstructions to quantify changes in wind stress between Pliocene and modern conditions. Ocean temperatures are specified, while land temperatures are allowed to evolve according to local energy balance. We find that both SST reconstructions result in reduced upwelling-favorable winds around all four midlatitude upwelling sites, suggesting that the significant coastal warm anomalies could be a secondary consequence of whatever sets the large-scale low-gradient SST pattern. We also show that coastal upwelling responds differently to Pliocene boundary conditions than near-coast large-scale curl-driven upwelling and point out that this may account for the decoupling of SST and productivity in the proxy record [Lawrence *et al.*, 2006; Dekens *et al.*, 2007].

2. Model Description and Experimental Setup

We use the National Center for Atmospheric Research Community Atmosphere Model (CAM) version 5.1.1 [Neale *et al.*, 2012]. This is the atmospheric component of the Community Earth System Model version 1.0.4, run with prescribed sea surface temperatures and sea ice, $0.9^\circ \times 1.25^\circ$ horizontal resolution, and 30 levels in the vertical.

We present three primary simulations, each based on a different SST distribution (Figure 1). The control case uses a modern (1982–2001) SST climatology from the Hadley Centre Sea Ice and Sea Surface Temperature (HadISST) data set [Rayner *et al.*, 2003]. The first Pliocene case employs the Pliocene Reconstruction Interpretation and Synoptic Mapping (PRISM) 3-D data set, a reconstruction of global ocean temperatures during the mid-Piacenzian (3.29 Ma to 2.97 Ma) developed by the U.S. Geological Survey Pliocene Reconstruction Interpretation and Synoptic Mapping (PRISM) group [Dowsett *et al.*, 2009]. This is the latest version of an ongoing effort to provide lower boundary conditions for Pliocene modeling studies, incorporating all available proxy records [Dowsett and Poore, 1991; Dowsett *et al.*, 1996; Dowsett and Robinson, 2009; Dowsett *et al.*, 2013]. The PRISM 3-D SST reconstruction incorporates geochemical (alkenone and Mg/Ca) and foraminiferal assemblage data from 86 sediment core sites, which are listed in Dowsett *et al.* [2009]. The Pliocene ocean circulation is

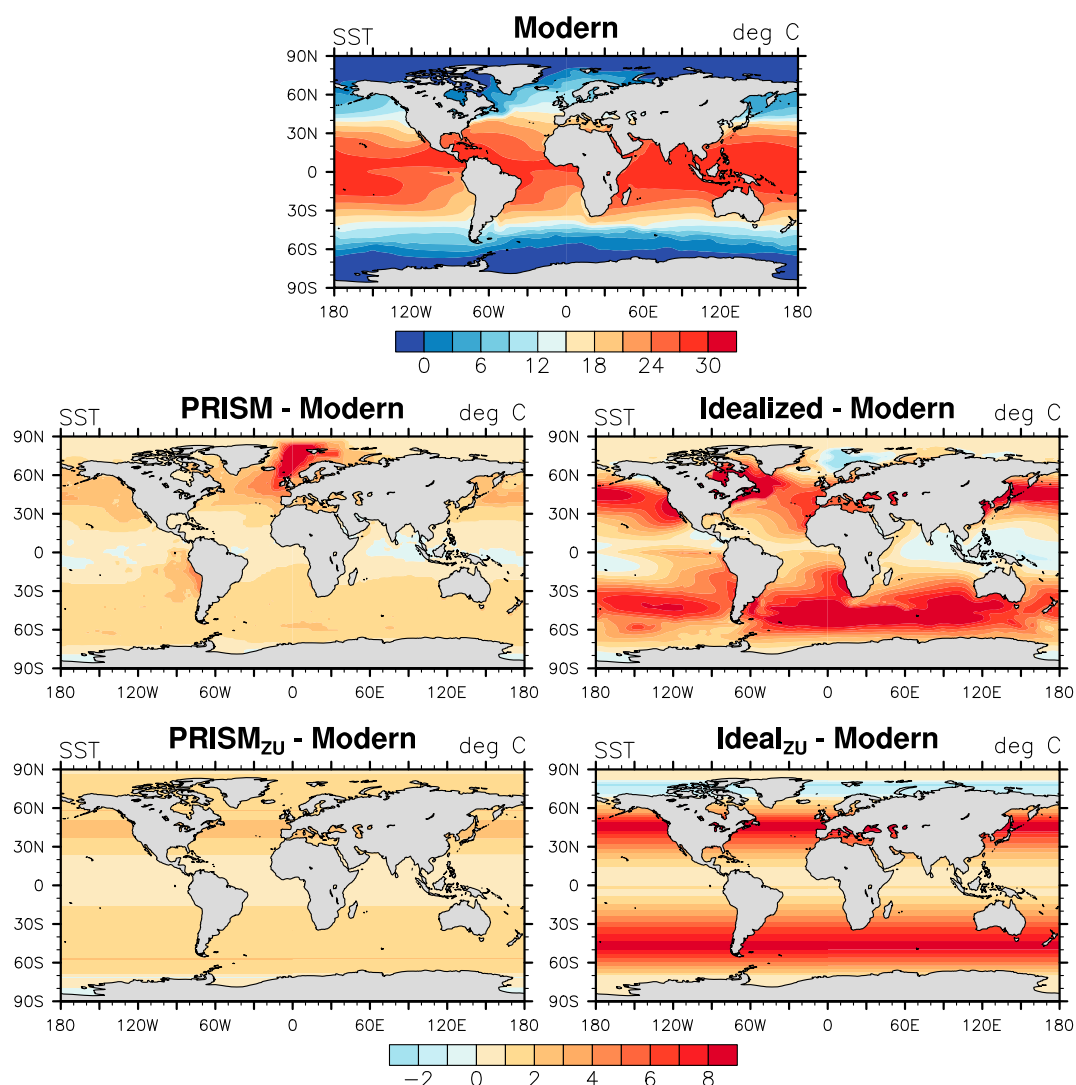


Figure 1. The annual mean sea surface temperatures (SSTs) used in the (top) modern simulation and SST anomalies used in the (middle left) PRISM3, (middle right) idealized, (bottom left) PRISM_{ZU}, and (bottom right) ideal_{ZU} simulations. Black dots indicate sediment core sites listed in section 3.

assumed to be similar to modern, and the Pliocene SST map is subjectively constructed using present-day SST and the proxy data as guides. This reconstruction is mainly limited by a lack of spatial coverage by proxy data, which, for example, do not cover the central Pacific.

The second Pliocene case uses an idealized SST reconstruction by *Brierley et al.* [2009], in which the tropical warm pool is extended poleward and zonal gradients are nearly eliminated. This is based on alkenone and Mg/Ca data at 15 sites during an earlier period (4–4.2 Ma) than the PRISM interval, sometimes called the Pliocene Thermal Optimum. Differences from modern SSTs are larger than in the PRISM3 reconstruction, and this case may be viewed as an extreme limit of the generally low-gradient conditions which seem to have prevailed throughout the Pliocene. This reconstruction relies heavily on assumptions about the relative SST gradients in the Pliocene ocean. For example, mid-Pacific temperatures are reasonably assumed to lie between temperatures in the equatorial warm pool and those in the California upwelling zone. The significant Pliocene SST anomalies off California then imply warmer temperatures across the Pacific. Small offsets are added to account for the North Atlantic being generally cooler than the North Pacific, the south Atlantic being warmer than the South Pacific, and upwelling regions being cooler than surrounding waters. A crude seasonal cycle is included by shifting the SST profile in latitude. Equations precisely describing this distribution, as well as the sediment core sites it is based on, are available in the supporting information of *Brierley et al.* [2009].

Table 1. Simulation Descriptions

Model Run	Description
Modern	SST climatology from HadISST, 355 ppm CO ₂ , modern topography, and land surface
PRISM	As in Modern but using PRISM3 Pliocene SST and 405 ppm CO ₂
Idealized	As in Modern but using idealized Pliocene SST and 405 ppm CO ₂
PRISM _{ZU}	As in PRISM but using zonally uniform Pliocene SST anomalies
Ideal _{ZU}	As in Idealized but using zonally uniform Pliocene SST anomalies
PRISM _T	As in PRISM but also using Pliocene topography
PRISM _{TL}	As in PRISM _T but also using Pliocene land surface types

Sea ice in the modern case is taken from the HadISST climatology, and in the PRISM case is taken from the PRISM3D reconstruction. In the idealized case, sea ice fraction is specified at 90% wherever the SST drops below freezing. Though this is simplistic, we have found in separate tests that changes in the surface winds around midlatitude upwelling sites are relatively insensitive to the sea ice distribution. Atmospheric CO₂ concentrations were set to 355 ppm in the modern case, and 405 ppm in the Pliocene simulations as recommended by the Pliocene Model Intercomparison Project [Haywood *et al.*, 2010] and consistent with recent estimates [Pagani *et al.*, 2010; Seki *et al.*, 2010]. Orbital parameters, methane, ozone, and atmospheric aerosols are set to modern (1981–2001) climatological values in all simulations. Each simulation is run for 21 years, and the first year is discarded to allow for model equilibration. Monthly values from the remaining 20 years are used for the calculations shown here. Trends in global mean land surface temperature over years 2–11 of the PRISM and idealized simulations are less than 0.01°C per year, and no single year deviates more than 0.2°C from the 10 year mean, indicating they are near equilibrium after the first year.

The primary simulations are supplemented by two runs, denoted PRISM_{ZU} and Ideal_{ZU}, in which Pliocene SST anomalies are zonally uniform and only a function of latitude. That is

$$SST_{\text{PlioZU}} = SST_{\text{Modern}} + \overline{SST_{\text{Plio}} - SST_{\text{Modern}}}^{x,t}, \quad (1)$$

where the overbar indicates an average over all longitudes and months. These simulations serve to separate the effect of the large-scale meridional SST gradient from local SST in the upwelling zones, as discussed below. The CO₂ concentrations and other model parameters are identical to their values in the primary Pliocene runs.

The above simulations use modern topography and land surface characteristics, but we also examine the sensitivity of coastal winds to Pliocene topography and land surface types. Topography can influence surface winds, and land surface properties can affect surface albedo and heat and moisture fluxes, which in turn affect the land-sea temperature contrast, pressure gradient, and wind field. We conduct two tests, one with Pliocene topography, and another with both Pliocene topography and surface biome and land ice. Both tests are run with PRISM3 SST, and the Pliocene topography and surface properties are taken from the PRISM3D data set. All of the above simulations are summarized in Table 1.

We note briefly that the modern, PRISM, and idealized simulations were repeated using CAM4, with similar relative reductions in coastal wind stress and wind stress curl. This suggests that the basic response is insensitive to the model configuration.

3. Results

Wind-driven upwelling around all four sites can be broken into two processes. Near the coast, wind stress parallel to the coastline drives a net transport of surface water away from the coast, which is replaced by colder water from below. A linear approximation for the coastal upwelling mass flux can be derived from the momentum and mass conservation equations [cf., Marshall and Plumb, 2008],

$$M_{\text{coast}} = \frac{\tau_{\text{as}}}{f}, \quad (2)$$

where τ_{as} is the alongshore component of surface wind stress, and f is the coriolis parameter. This yields the upwelled mass for a given length of coastline, with units of $\text{kg s}^{-1} \text{m}^{-1}$. Away from the coast, offshore upwelling can occur due to spatial variations in wind stress

$$M_{\text{curl}} = \frac{1}{f} \nabla \times \vec{\tau}, \quad (3)$$

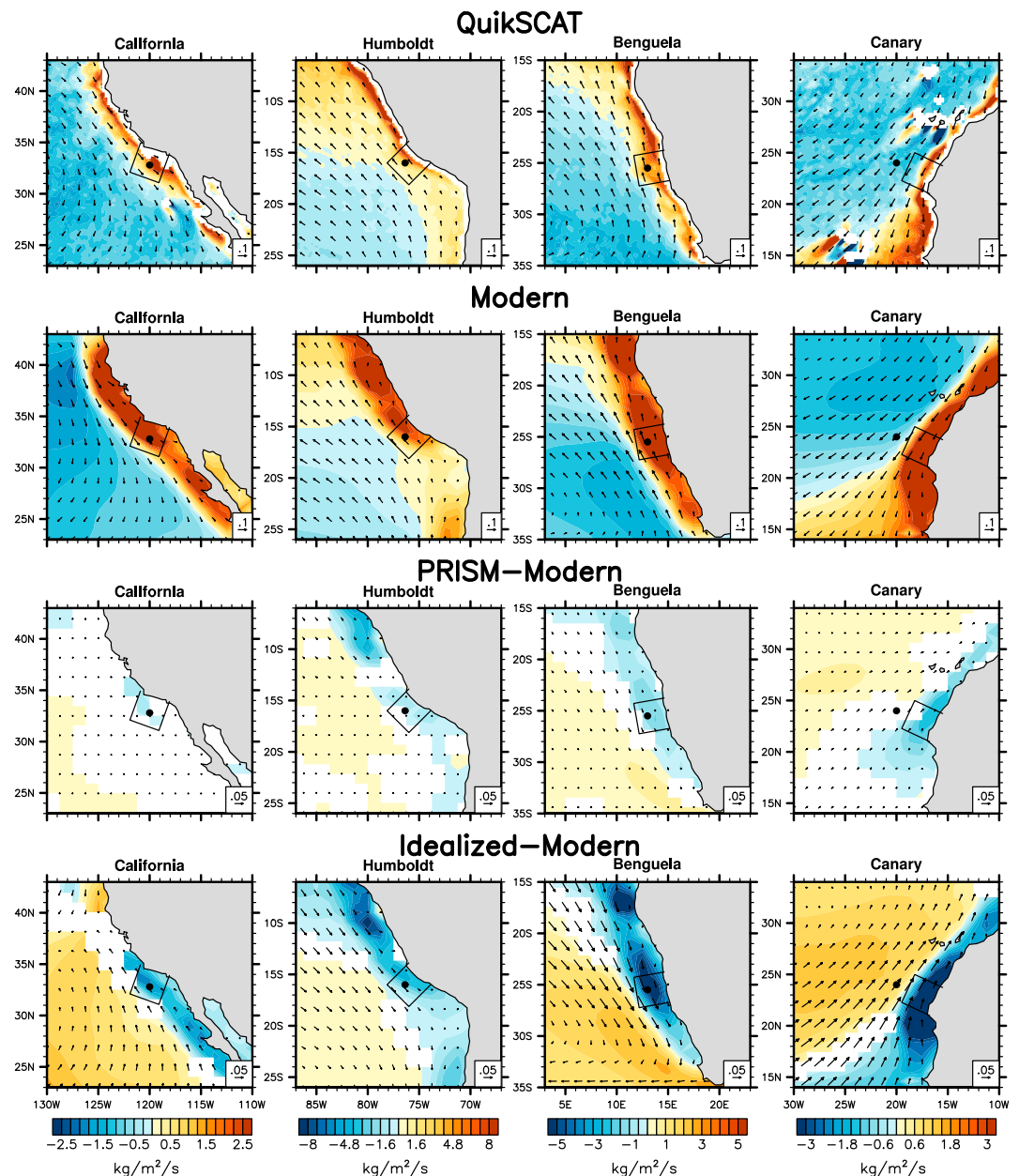


Figure 2. Annual mean surface wind stress (vectors) and upwelling due to wind stress curl (contours). Shown are (first row) QuikSCAT satellite observations, the CAM5 simulation with (second row) modern SST, the (third row) difference between PRISM3 and Modern SST, and the (fourth row) difference between idealized and modern SST. Upwelling units are kg/m²/s, with a shared color scale for each site. Statistically insignificant differences appear white. A 0.1 N/m² (QuikSCAT and modern) or 0.05 N/m² (differences) reference vector is shown in the bottom right of each panel. The model is able to reproduce the general observed patterns of wind stress curl and simulates reductions in curl when run with estimates of Pliocene SST.

where $\nabla \times$ is the curl operator and $\vec{\tau}$ is the surface wind stress vector. This is the upwelling mass flux per unit area in kg s⁻¹ m⁻¹. The alongshore wind stress and wind stress curl are widely used in studies of upwelling variability and trends in eastern boundary current regions [e.g., Bakun and Nelson, 1991].

Surface wind stress around upwelling sites in the CAM5 modern case is first validated against a climatology of QuikSCAT satellite observations from 2000 to 2009 on a 0.25°×0.25° grid. The observed wind velocities are converted to surface stresses using a bulk formula. In general the agreement is quite good. Contours in Figure 2 show the upwelling mass flux per unit area inferred from the wind stress curl using equation (2), while

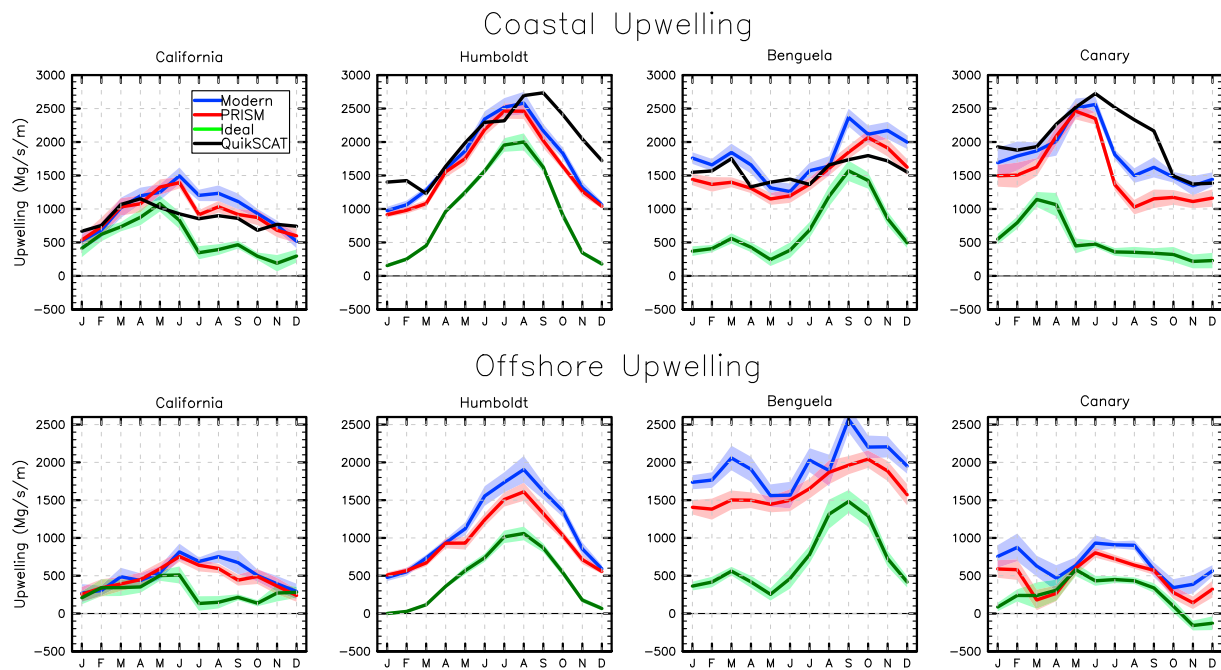


Figure 3. Monthly indices for coastal and curl-driven upwelling around each sediment core site, for the modern (blue), PRISM (red) and idealized (green) cases, and for QuikSCAT satellite observations (black). Upwelling inferred from (top row) alongshore wind stress and (bottom row) wind stress curl is reduced when the model is run with Pliocene SST. Indices are based on average alongshore wind stress (coastal) or wind stress curl (offshore) within a 300 km square box around each sediment core site, as indicated in Figure 2. Shading indicates ± 1 standard error.

the vectors indicate surface wind stress. The model is able to reproduce the large-scale pattern and seasonality of wind stress and wind stress curl at all four locations, although the magnitude is generally overestimated. Other model deficiencies include a failure to capture the small-scale wind stress curl associated with the Canary Islands, and a wider-than-observed strip of positive curl along each coastline, likely due to the coarser model resolution. These should have only a minor effect on the large-scale changes which concern us.

The statistical significance of differences between the modern and Pliocene runs is evaluated using Student's *t* test, and values insignificant at the 0.05 level appear white in the difference plots. We find that PRISM3 SST results in modest reductions in wind stress curl and alongshore stress within the Canary and Benguela Current regions, and somewhat smaller reductions within the California and Humboldt Currents (Figure 2).

To assess the seasonality of upwelling changes, Figure 3 presents local seasonal indices of coastal and offshore upwelling taken from a single location in each upwelling region. To enable comparison with previous work, we center these indices on the four sediment core sites highlighted in *Dekens et al.* [2007]: Ocean Drilling Project (ODP) site 1014 in the California Current System, ODP site 958 in the Canary Current near the Western Sahara, ODP site 1237 in the Humboldt Current off the Peruvian coast, and ODP site 1084 in the Benguela Current near present-day Namibia. The indices are defined by identifying the nearest coastal point to each sediment core site and averaging all grid points within a box extending 150 km in each alongshore direction, and 300 km out to sea, as indicated in Figure 2. We find that nearby points produce qualitatively similar time series, and the indices generally reflect their upwelling region as a whole. With PRISM3 SST, the indices show reductions in both upwelling components of 5–20%, depending on site and season.

The spatial pattern of wind stress changes due to the idealized SST is similar to that of PRISM3, but the changes are generally of greater amplitude. This is consistent with the idealized SST anomalies being a more extreme version of the PRISM3 reconstruction. The idealized case also results in substantial reductions in alongshore wind stress at all four sites, often 50% or more.

Similar reductions are seen in the Pliocene simulations forced by zonally averaged SST anomalies, shown in Figure 4. The basic pattern of reduced upwelling near the coasts is reproduced around all four sites in both simulations. The magnitude of the reductions at most sites in the PRISM_{ZU} case is comparable to or larger than the reductions in the PRISM case, although the reductions in the Ideal_{ZU} case are somewhat weaker than with

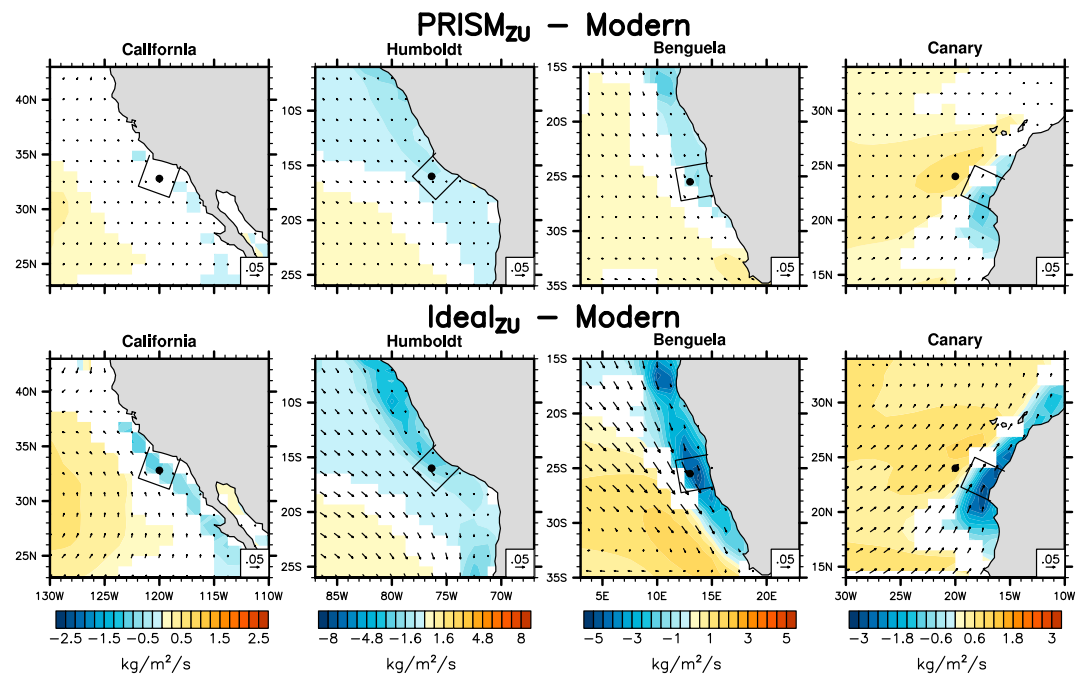


Figure 4. Difference in annual mean surface wind stress (vectors) and curl-driven upwelling mass flux (contours) between simulations with zonal and annual mean Pliocene SST anomalies and the modern case. Units as in the bottom of Figure 2. Statistically insignificant differences appear white.

idealized SST. This suggests that most of the reductions in upwelling favorable winds are due to the weakened large-scale meridional SST gradient, while the weakened zonal gradients have a smaller effect.

The weakened SST gradients affect midlatitude surface winds through at least two mechanisms, not entirely independent. First, the reduced pole-to-equator temperature gradient leads to a weakening of the Hadley circulation. This results in less subsiding air and a reduction in the strength of the subtropical highs, indicated in Figure 5. This reduces the land-sea pressure gradient and the associated alongshore winds. A weakening of the Hadley circulation has been reported in previous Pliocene modeling studies [e.g., Chandler *et al.*, 1994; Brierley *et al.*, 2009], although some models simulate a broadening of the circulation rather than a decrease in strength [e.g., Haywood *et al.*, 2000].

Second, the warmer prescribed midlatitude SST can directly reduce midlatitude land-sea temperature contrasts, which in turn weaken land-sea pressure gradients and coastal winds. The weaker temperature contrast may be partially due to the model configuration: we are prescribing sea surface temperatures, but allowing the land model to determine its own equilibrium, which depends on accurately specifying Pliocene land surface properties. The change in land-sea contrast could be overestimated in our results if either the prescribed SST were too high or the simulated land temperatures were too low. In that event, changes in surface winds would also be overestimated, along with changes in implied upwelling.

The modern land-sea contrast is reinforced by a number of positive feedbacks. For example, the combination of subsiding air and evaporation from the ocean surface produces low cloud decks over the eastern ocean regions, and the resulting high albedo contributes to relatively low surface temperatures, which in turn reinforce the subsidence regime. Since expansive low cloud decks are less prevalent over continents, a weakened Hadley circulation should reduce low cloud cover over the ocean more than over land, and the resulting radiative changes would support a reduced land-sea temperature difference. This cloud feedback is seen to a striking degree in our simulations. Figure 6 shows the change in low cloud fraction in the two Pliocene simulations relative to modern and the corresponding changes in shortwave cloud radiative forcing. Decreases in subtropical low clouds range from 10–20% in the PRISM case to 20–30% in the idealized case. Over oceans, the corresponding changes in surface radiative heating are of order +15 W/m² (PRISM) and +30 W/m² (Ideal), while over land both runs show small increases in cloud cover and a net cooling effect. This combination would strongly contribute to a weaker land-sea contrast. Differences in midlatitude clouds have been previously

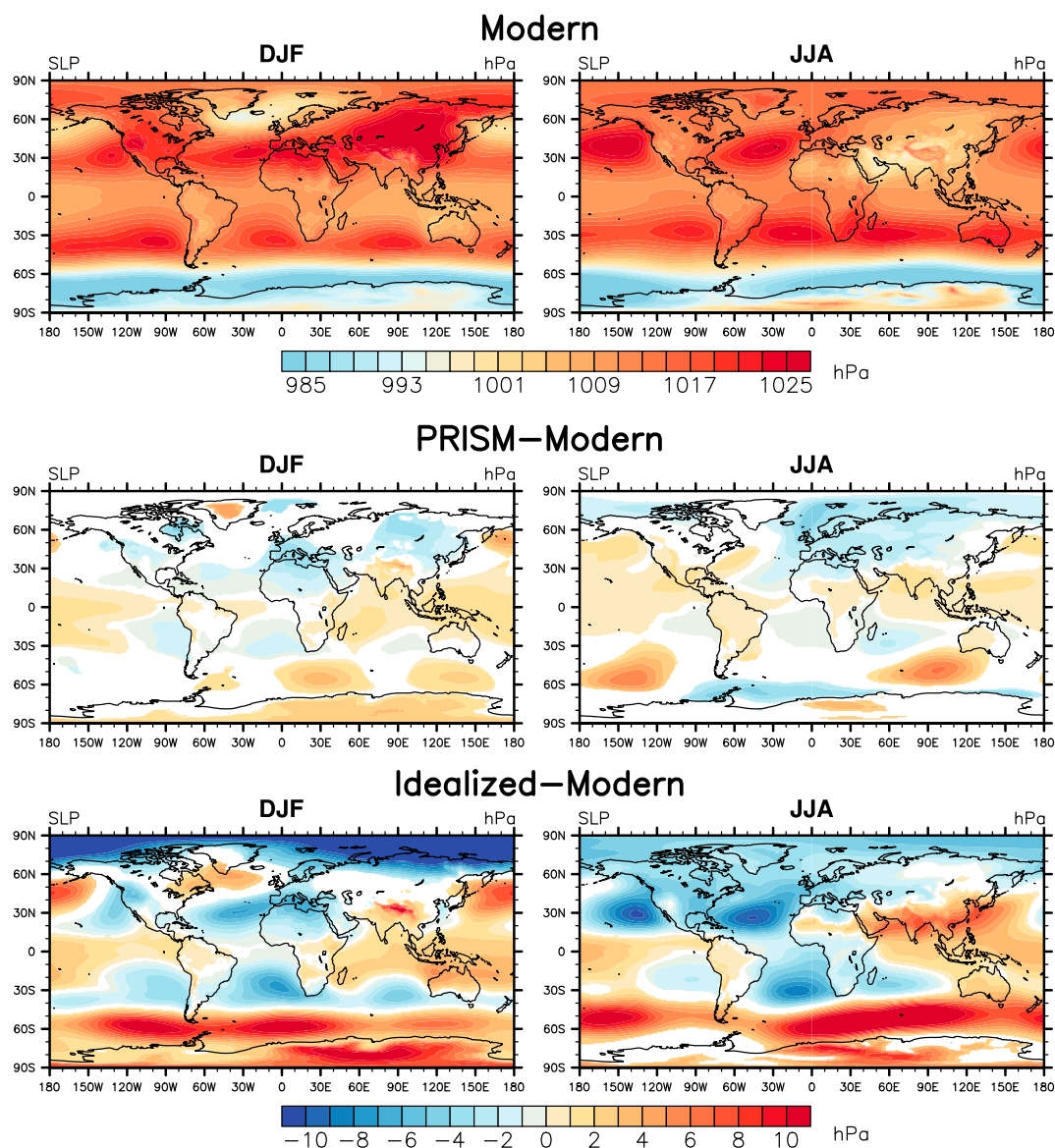


Figure 5. The annual mean sea level pressure (hPa) from the (top row) modern simulation and the differences between the modern and (middle row) PRISM, and (bottom row) idealized simulations. Both Pliocene simulations show reductions in the strength of the subtropical highs. Statistically insignificant differences appear white.

proposed as a mechanism to explain Pliocene SST anomalies [Barreiro and Philander, 2008; Burls and Fedorov, 2014], and the cloud reductions simulated here are consistent with that hypothesis.

The separate effects of Pliocene topography and land surface type are analyzed in Figure 7. The Pliocene boundary conditions include generally lower elevations in the Andes and Sierra-Nevada ranges and reduced ice sheet elevations over Greenland and Antarctica. The Pliocene topography makes little difference around the Atlantic sites, but the California and Humboldt regions both show spatially complex changes in wind stress with magnitudes comparable to those induced by the idealized SST. Wind stress curl is generally reduced off California, except within roughly 100 km of ODP site 1014, which sees a small increase. Changes in the Humboldt current show an alternating pattern of increases and decreases. The magnitude of these effects suggests that topography could potentially contribute to the SST anomalies at the Pacific sites, but the impacts may be local. Given that these effects change on the scale of a single model grid cell and are therefore not well resolved, we suggest that this pattern indicates the qualitative significance of topography but should not be taken literally. In contrast with topography, the wind stress changes associated with Pliocene land types are statistically insignificant around all four upwelling sites.

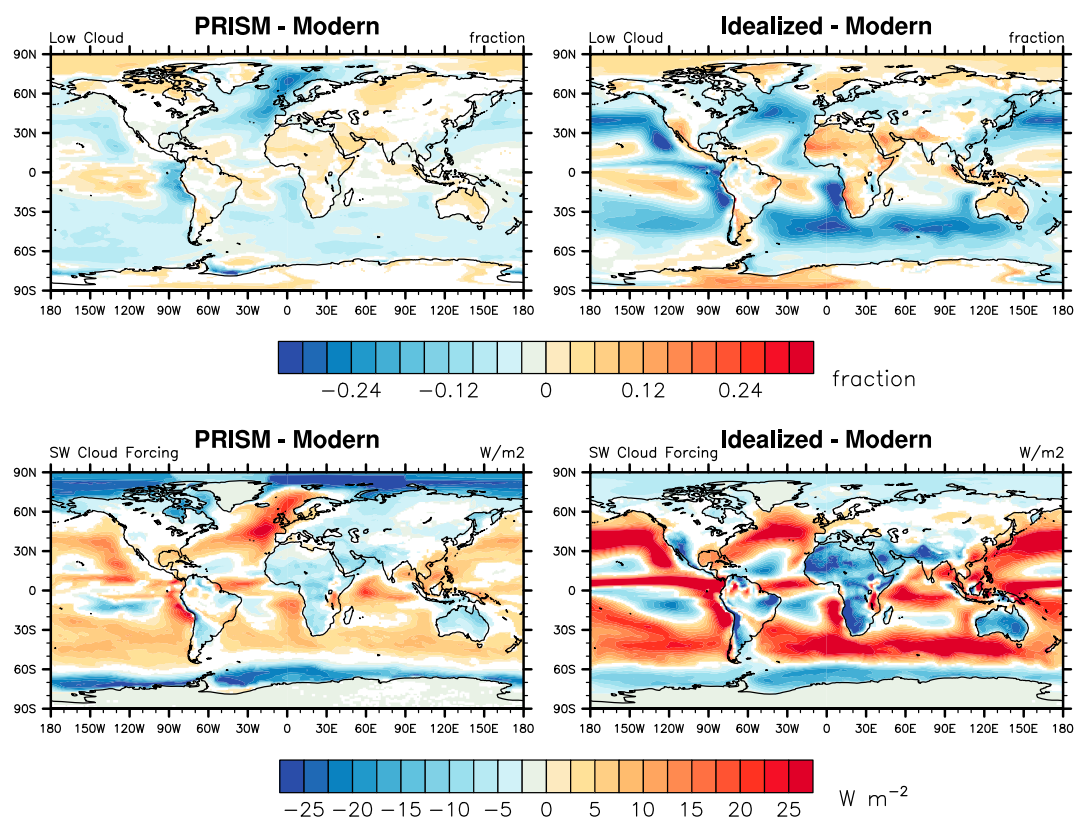


Figure 6. The annual mean difference in (top row) low cloud fraction and (bottom row) shortwave cloud radiative forcing between the (left column) PRISM and (right column) idealized cases, relative to modern. Statistically insignificant differences appear white.

Proxies for sea surface temperature and biological productivity are decoupled on secular timescales [e.g., Lawrence et al., 2006; Dekens et al., 2007]. This decoupling, along with indications of high productivity in the Pliocene, has led to arguments that Pliocene SST anomalies could not be due solely to changes in upwelling, and that changes in source water properties must play a significant role [e.g., Dekens et al., 2007]. While we agree that nonupwelling factors likely contributed to the warm anomalies, this argument may underestimate the role of wind stress. In particular, it requires a strong correlation between productivity and upwelling intensity on long timescales. However, if this were the case, the variability seen in productivity records would imply extreme and unrealistic changes in wind stress. It has been pointed out [e.g., Lawrence et al., 2006] that recorded productivity can be strongly influenced by nonupwelling factors, such as nutrient availability [e.g., Bolton et al., 2011; Lawrence et al., 2013], or nonlinearities, such as being skewed toward periods of high productivity. As such, secular variations in productivity could be due to nonupwelling factors, and high productivity does not necessarily indicate stronger winds.

Here we suggest an additional factor that could contribute to the decoupling of SST and productivity, based on the differing effects of offshore and coastal upwelling. Unlike coastal upwelling, the effects of wind stress curl are generally too weak to upwell nutrient-rich deeper water but can still affect SST by upwelling from shallower depths. If alongshore wind stress and offshore wind stress curl were to vary independently over time, this could produce independent histories of SST and productivity, even though variations in both are derived from the changing wind field.

To illustrate this idea, we ran five simulations in which PRISM3 SST, topography, and land surface anomalies (relative to modern) are scaled from 0 to 1, such that 0 corresponds to modern conditions, 1 to Pliocene conditions, and intermediate values may be thought of as crudely representing the temporal evolution between these two states over the last 3 Ma. Figure 8 shows annual mean values of the coastal and offshore upwelling indices from these runs, with the modern case denoted by a red asterisk. A linear relationship between the two indices would have indicated that they respond similarly, proportional to one another, to the changing

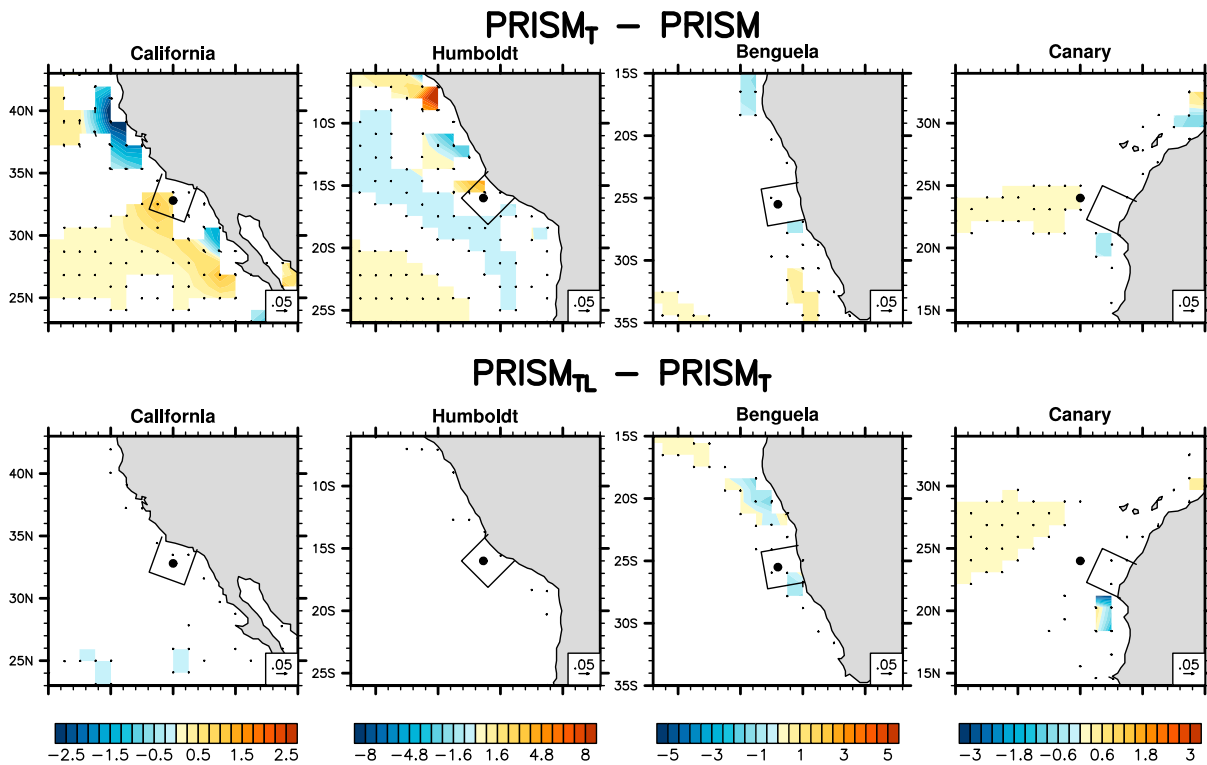


Figure 7. Differences in annual mean surface wind stress (vectors) and upwelling due to wind stress curl (contours) between simulations with Pliocene and modern topography ((top row) $PRISM_T - PRISM$). Below are differences between simulations with Pliocene surface types, and Pliocene topography only ((bottom row) $PRISM_{TL} - PRISM_T$). All simulations use PRISM SST. Upwelling units are $kg/m^2/s$, with a shared color scale for each site. Statistically insignificant differences appear white. A $0.05 N/m^2$ reference vector is shown in the bottom right of each panel. Pliocene topography has a significant effect on surface wind around the Pacific sites, while the effects of Pliocene land type are largely insignificant.

boundary conditions. However, their nonlinear path demonstrates that independent histories of coastal and offshore upwelling can occur as the SST, CO_2 , and land surface gradually transition from Pliocene to modern conditions. Given that the two upwelling mechanisms influence SST and productivity differently, this suggests that the decoupling of SST and productivity seen in the proxy record could result in part from the differing sensitivities of offshore and coastal upwelling to changing boundary conditions. These simulations are only intended as a proof of concept that independent histories are possible. A full evaluation of this hypothesis will require a more sophisticated approach to relate productivity indicators with upwelling strength.

As cautionary notes to the above results, we point out that the model grid used here, while relatively high resolution, is not fine enough to capture the small-scale effects of local topography, which can account for a significant component of wind stress curl. For example, the protrusion of the California coastline at

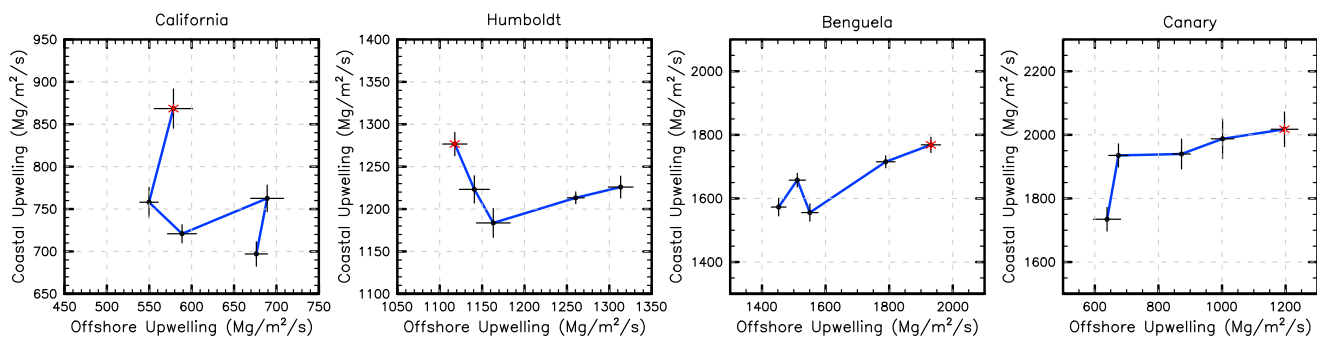


Figure 8. Annual mean coastal and offshore upwelling indices for the modern run (red asterisk) and four simulations in which PRISM3 SST, topography, and land surface anomalies are scaled from 0.25 to 1. Demonstrates a hypothetical evolution over time in which coastal and offshore upwelling do not covary. Crosses indicate ± 1 standard error.

Point Conception is associated with enhanced wind stress curl and upwelling in the Southern California bight [Pickett, 2003]. Winant and Dorman [1997] found that going from 1° to 0.2° resolution increases the observed wind stress curl off California by a factor of 3. Mesoscale variations in sea surface temperature are also known to modulate the local wind speed and thereby the upwelling [Boé *et al.*, 2011]. It is possible that small-scale effects could have differed significantly between the Pliocene and the present, given changes in sea level and coastal topography, though it is unclear if this would increase or decrease upwelling systematically. Insufficient model resolution could also account for the lack of change in upwelling and coastal SST in coupled simulations of the Pliocene. For example, the PlioMIP CCSM4 used horizontal model grid spacing of roughly 1° [Rosenbloom *et al.*, 2013], which is known to reduce the strength of upwelling [Gent *et al.*, 2010]. If upwelling in present-day simulations is too weak, then simulated Pliocene anomalies would necessarily be small.

4. Summary and Conclusions

Simulations with the global Community Atmosphere Model (CAM5) [Neale *et al.*, 2012] demonstrate that two different reconstructions of Pliocene sea surface temperatures imply reductions in upwelling-favorable wind around the four major eastern boundary current regions. Use of the mid-Piacenzian (3.29–2.97 Ma) SST reconstruction developed by the PRISM group results in reductions of 10–20% in the Canary and Benguela current systems, and smaller reductions of 5–10% in the California and Humboldt systems. An idealized reconstruction of the earlier Pliocene warm period (4–4.2 Ma) results in larger reductions of 20–50%, depending on season. In both scenarios, changes in wind stress are driven by the combination of a general weakening of the Hadley circulation and a reduction in the land-sea temperature contrast. It was also argued that the decoupling of SST and productivity in the proxy record does not rule out wind-induced upwelling changes. Gradually varying the prescribed large-scale SST, topography and land surface characteristics between Pliocene and modern values were found to produce independent changes in implied coastal and offshore upwelling, which could in turn produce differing histories of SST and productivity within upwelling zones. These results suggest that at least part of the warm anomalies found at Pliocene coastal sediment core sites may be attributed to wind-driven reductions in upwelling intensity. Quantifying the local importance of wind stress changes will require further work, perhaps with regional ocean models.

The Pliocene is often presented as an instructive analogue for future global warming [e.g., Chandler *et al.*, 1994; Dowsett and Robinson, 2009; Salzmann *et al.*, 2009; although see Lunt *et al.*, 2009], and the reduced upwelling in these simulations has long-term implications for coastal climate. However, lessons for upwelling systems may not apply immediately. The Pliocene coastal warm anomalies persisted for 2–3 My [Herbert and Schuffert, 1998; Marlow *et al.*, 2000; Dekens *et al.*, 2007], and like the results presented here, represent a state of relative equilibrium. Changes in upwelling over the next few decades, though, are expected to be driven by transient effects. Bakun [1990] hypothesized that the different rates of warming over land and ocean would lead to an increased land-sea surface pressure gradient, stronger geostrophic surface winds along the coast, and thus a transient increase in upwelling. This prediction is supported by observed trends in wind stress near all four major upwelling systems [Narayan *et al.*, 2010] and by direct indicators of productivity and cooler temperatures off Peru [Gutiérrez *et al.*, 2011]. Interestingly, surface temperatures off California have increased slightly due to a deepening of the thermocline [Lorenzo and Miller, 2005], but this seems to be a local change.

References

- Bakun, A. (1990), Global climate change and intensification of coastal ocean upwelling, *Science*, 247(4939), 198–201.
- Bakun, A., and C. S. Nelson (1991), The seasonal cycle of wind-stress curl in subtropical eastern boundary current regions, *J. Phys. Ocean.*, 21, 1815–1834.
- Barreiro, M., and S. G. Philander (2008), Response of the tropical Pacific to changes in extratropical clouds, *Clim. Dyn.*, 31(6), 713–729.
- Boccaletti, G., R. C. Pacanowski, S. G. H. Philander, and A. V. Fedorov (2004), The thermal structure of the upper ocean, *J. Phys. Ocean.*, 34, 888–902.
- Boé, J., A. Hall, F. Colas, J. C. McWilliams, X. Qu, J. Kurian, and S. B. Kapnick (2011), What shapes mesoscale wind anomalies in coastal upwelling zones?, *Clim. Dyn.*, 36(11–12), 2037–2049.
- Bolton, C. T., K. T. Lawrence, S. J. Gibbs, P. A. Wilson, and T. D. Herbert (2011), Biotic and geochemical evidence for a global latitudinal shift in ocean biogeochemistry and export productivity during the late Pliocene, *Earth and Planet. Sci. Lett.*, 308, 200–210.
- Brierley, C. M., A. V. Fedorov, Z. Liu, T. D. Herbert, K. T. Lawrence, and J. P. LaRiviere (2009), Greatly expanded tropical warm pool and weakened Hadley circulation in the early Pliocene, *Science*, 323(5922), 1714–1718.
- Burls, N. J., and A. V. Fedorov (2014), Simulating Pliocene warmth and a permanent El Niño state: The role of cloud albedo, *Paleoceanography*, 29, 893–910, doi:10.1002/2014PA002644.
- Chaisson, W. (1995), Planktonic foraminiferal assemblages and paleoceanographic change in the trans-tropical Pacific Ocean: A comparison of west (Leg 130) an east (Leg 138), latest Miocene to Pleistocene, *Proc. Ocean Drill. Program Sci. Results*, 138, 555–597.

Acknowledgments

We thank C. Ravelo for helpful discussions, in particular on the different roles of coastal and large-scale curl-driven upwelling in influencing productivity and surface temperature. This work was supported by an NSF Graduate Research Fellowship (NPA) and NSF Climate Dynamics grants ATM-0902844 P2C2 and ATM-0754332 (ET). E.T. thanks the Weizmann Institute for its hospitality during parts of this work. Model computations were run on the Odyssey cluster supported by the FAS Science Division Research Computing Group at Harvard University. QuikSCAT data were produced by Remote Sensing Systems and sponsored by the NASA Ocean Vector Winds Science Team. Model output is available by request, email NPA at nathan.arnold@nasa.gov.

- Chandler, M., D. Rind, and R. Thompson (1994), Joint investigations of the middle Pliocene climate II: GISS GCM Northern Hemisphere results, *Global Planet. Change*, *9*, 197–219.
- Dekens, P. S., A. C. Ravelo, and M. D. McCarthy (2007), Warm upwelling regions in the Pliocene warm period, *Paleoceanography*, *22*, PA3211, doi:10.1029/2006PA001394.
- Dekens, P. S., A. C. Ravelo, M. D. McCarthy, and C. A. Edwards (2008), A 5 million year comparison of Mg/Ca and alkenone paleothermometers, *Geochem. Geophys. Geosyst.*, *9*, Q10001, doi:10.1029/2007GC001931.
- Dowsett, H., J. Barron, and R. Poore (1996), Middle Pliocene sea surface temperatures: A global reconstruction, *Mar. Micropaleontol.*, *27*, 13–25.
- Dowsett, H. J., and T. M. Cronin (1990), High eustatic sea level during the middle Pliocene: Evidence from the southeastern U.S. Atlantic Coastal Plain, *Geology*, *18*, 435–438.
- Dowsett, H. J., and R. Poore (1991), Pliocene sea surface temperatures of the North Atlantic ocean at 3.0 Ma, *Quat. Sci. Rev.*, *10*, 189–204.
- Dowsett, H. J., and M. M. Robinson (2009), Mid-Pliocene equatorial Pacific sea surface temperature reconstruction: A multi-proxy perspective, *Philos. Trans. R. Soc. A*, *367*, 109–125.
- Dowsett, H. J., M. M. Robinson, and K. M. Foley (2009), Pliocene three-dimensional global ocean temperature reconstruction, *Clim. Past Discuss.*, *5*(4), 1901–1928.
- Dowsett, H. J., A. M. Haywood, P. J. Valdes, M. M. Robinson, D. J. Lunt, D. J. Hill, D. K. Stoll, and K. M. Foley (2011), Sea surface temperatures of the mid-Piacenzian warm period: A comparison of PRISM3 and HadCM3, *Paleogeog. Paleoclim. Paleoeco.*, *309*, 83–91.
- Dowsett, H. J., et al. (2012), Assessing confidence in Pliocene sea surface temperatures to evaluate predictive models, *Nat. Clim. Change*, *2*, 365–371.
- Dowsett, H. J., et al. (2013), Sea surface temperature of the mid-Piacenzian ocean: A data-model comparison, *Sci. Rep.*, *3*, 1–8, doi:10.1038/srep02013.
- Fedorov, A. V., R. Pacanowski, S. G. Philander, and G. Boccaletti (2004), The effect of salinity on the wind-driven circulation and the thermal structure of the upper ocean, *J. Phys. Ocean.*, *34*, 1949–1966.
- Fedorov, A. V., P. S. Dekens, M. McCarthy, A. C. Ravelo, P. B. deMenocal, M. Barriero, R. C. Pacanowski, and S. G. Philander (2006), The Pliocene paradox (mechanisms for a permanent El Niño), *Science*, *312*, 1485–1489.
- Fedorov, A. V., C. M. Brierley, and K. Emanuel (2010), Tropical cyclones and permanent El Niño in the early Pliocene epoch, *Nature*, *463*(7284), 1066–70.
- Fedorov, A. V., C. M. Brierley, K. T. Lawrence, Z. Liu, P. S. Dekens, and A. C. Ravelo (2013), Patterns and mechanisms of early Pliocene warmth, *Nature*, *496*, 43–52.
- Gent, P. R., S. G. Yeager, R. B. Neale, S. Levis, and D. A. Bailer (2010), Improvements in a half degree atmosphere/land version of the CCSM, *Clim. Dyn.*, *34*(6), 819–833.
- Groeneveld, J., S. Steph. R. Tiedemann, D. Garbe-Schönberg, D. Nurnberg, and A. Sturm (2006), Pliocene mixed-layer oceanography for site 1241, using combined Mg/Ca and $\delta^{18}O$ analyses of Globigerinoides Sacculifer, in *Proceedings of the Ocean Drilling Program, Scientific Results*, vol. 202, edited by R. Tiedemann et al., pp. 1–27, Ocean Drilling Program, College Station, Tex.
- Gutiérrez, D., et al. (2011), Coastal cooling and increased productivity in the main upwelling zone off Peru since the mid-twentieth century, *Geophys. Res. Lett.*, *38*, L07603, doi:10.1029/2010GL046324.
- Haywood, A. M., P. J. Valdes, and B. W. Sellwood (2000), Global scale palaeoclimate reconstruction of the middle Pliocene climate using the UKMO GCM: Initial results, *Global Planet. Change*, *25*, 239–256.
- Haywood, A. M., et al. (2010), Pliocene Model Intercomparison Project (PlioMIP): Experimental design and boundary conditions (Experiment 1), *Geosci. Model Develop.*, *3*(1), 227–242.
- Haywood, A. M., et al. (2012), Large-scale features of Pliocene climate: Results from the Pliocene Model Intercomparison Project, *Clim. Past Discuss.*, *8*(4), 2969–3013.
- Herbert, T. D., and J. D. Schuffert (1998), Alkenone unsaturation estimates of late Miocene through late Pliocene sea surface temperatures at site 958, *Proc. Ocean Drill. Program Sci. Results*, *159T*, 17–21.
- Lawrence, K. T., D. M. Sigman, T. D. Herbert, C. A. Riihimaki, C. T. Bolton, A. Martinez-Garcia, A. Rosell-Mele, and G. H. Haug (2013), Time-transgressive North Atlantic productivity changes upon Northern Hemisphere glaciation, *Paleoceanography*, *28*, 720–751, doi:10.1002/2013PA002546.
- Lawrence, K. T., Z. Liu, and T. D. Herbert (2006), Evolution of the eastern tropical Pacific through Plio-Pleistocene glaciation, *Science*, *312*(79), 79–83.
- Lorenzo, D. I., and A. J. Miller (2005), The warming of the California current system: Dynamics and ecosystem implications, *J. Phys. Oceanogr.*, *35*, 336–362.
- Lunt, D. J., A. M. Haywood, G. L. Foster, and E. J. Stone (2009), The Arctic cryosphere in the mid-Pliocene and the future, *Philos. Trans. R. Soc. A*, *367*, 49–67.
- Mann, K., and J. Lazier (2005), *Dynamics of Marine Ecosystems: Biological-Physical Interactions in the Oceans*, 3rd ed., Wiley-Blackwell, Oxford, U. K.
- Marlow, J. R., C. B. Lange, G. Wefer, and A. Rosell-Mele (2000), Upwelling intensification as part of the Pliocene-Pleistocene climate transition, *Science*, *290*(5500), 2288–2291.
- Marshall, J., and A. Plumb (2008), *Atmosphere, Ocean and Climate Dynamics*, Academic Press, Cambridge, Mass.
- Miller, K. G., J. D. Wright, J. V. Browning, A. K. Kulpeck, M. Kominz, T. R. Naish, B. S. Cramer, Y. Rosenthal, W. R. Peltier, and S. Sosdian (2012), High tide for the warm Pliocene: Implications of global sea level for Antarctic deglaciation, *Geology*, *40*(5), 407–410.
- Martinez-Botí, M. A., G. L. Foster, T. B. Chalk, E. J. Rohling, P. F. Sexton, D. J. Lunt, R. D. Pancost, M. P. S. Badger, and D. N. Schmidt (2015), Plio-Pleistocene climate sensitivity evaluated using high-resolution CO₂ records, *Nature*, *518*(7537), 49–54.
- Narayan, N., A. Paul, S. Mulitza, and M. Schulz (2010), Trends in coastal upwelling intensity during the late 20th century, *Ocean Sci.*, *6*(3), 815–823.
- Neale, R. B., et al. (2012), Description of the NCAR Community Atmosphere Model (CAM 5.0), *NCAR Tech. Note NCAR/TN-4861STR*, 289 pp. [Available online at http://www.cesm.ucar.edu/models/cesm1.0/cam/docs/description/cam5_desc.pdf]
- O'Brien, C. L., G. L. Foster, M. A. Martínez-Botí, R. Abell, J. W. B. Rae, and R. D. Pancost (2014), High sea surface temperatures in tropical warm pools during the Pliocene, *Nat. Geosci.*, *7*, 606–611.
- Pagani, M., Z. Liu, J. LaRiviere, and A. C. Ravelo (2010), High Earth-system climate sensitivity determined from Pliocene carbon dioxide concentrations, *Nat. Geosci.*, *3*(1), 27–30.
- Pauly, D., and V. Christensen (1995), Primary production required to sustain global fisheries, *Nature*, *374*, 255–257.
- Pickett, M. H. (2003), Ekman transport and pumping in the California Current based on the U.S. Navy's high-resolution atmospheric model (COAMPS), *J. Geophys. Res.*, *108*(C10), 3327–3337, doi:10.1029/2003JC001902.

- Pollard, D., and R. M. DeConto (2009), Modelling West Antarctic ice sheet growth and collapse through the past five million years, *Nature*, *458*(7236), 329–332.
- Ravelo, A. C., P. S. Dekens, and M. McCarthy (2006), Evidence for El Niño-like conditions during the Pliocene, *Geol. Soc. Am. Today*, *16*(3), 4–11.
- Raymo, M., B. Grant, M. Horowitz, and G. Rau (1996), Mid-Pliocene warmth: Stronger greenhouse and stronger conveyor, *Mar. Micropaleontol.*, *27*, 313–326.
- Raymo, M., J. X. Mitrovica, M. J. O'Leary, R. M. DeConto, and P. J. Hearty (2011), Departures from eustasy in Pliocene sea-level records, *Nat. Geosci.*, *4*, 328–332.
- Rayner, N., D. Parker, E. Horton, C. Folland, L. Alexander, D. Rowell, E. Kent, and A. Kaplan (2003), Global analyses of sea surface temperature, sea ice, and night marine air temperature since the late nineteenth century, *J. Geophys. Res.*, *108*(D14), 4407, doi:10.1029/2002JD002670.
- Rosenbloom, N. A., B. L. Otto-Bliesner, E. C. Brady, and P. J. Lawrence (2013), Simulating the mid-Pliocene warm period with the CCSM4 model, *Geosci. Model Dev.*, *6*, 549–561.
- Rovere, A., M. E. Raymo, J. X. Mitrovica, P. J. Hearty, M. J. O'Leary, and J. D. Inglis (2014), The mid-Pliocene sea-level conundrum: Glacial isostasy, eustasy and dynamic topography, *Earth and Planet. Sci. Lett.*, *387*, 27–33.
- Salzmann, U., A. Haywood, and D. Lunt (2009), The past is a guide to the future? Comparing Middle Pliocene vegetation with predicted biome distributions for the twenty-first century, *Philos. Trans. R. Soc. A*, *367*, 189–204.
- Scherer, R. P. (1991), Quaternary and Tertiary microfossils from beneath Ice Stream B: Evidence for a dynamic West Antarctic ice sheet history, *Paleogeog. Paleoclim. Paleoeco.*, *90*, 395–412.
- Seki, O., G. L. Foster, D. N. Schmidt, A. Mackensen, K. Kawamura, and R. D. Pancost (2010), Alkenone and boron-based Pliocene pCO₂ records, *Earth Planet. Sci. Lett.*, *292*(1–2), 201–211.
- Snyder, M. A., L. C. Sloan, N. S. Diffenbaugh, and J. L. Bell (2003), Future climate change and upwelling in the California Current, *Geophys. Res. Lett.*, *30*(15), 1823, doi:10.1029/2003GL017647.
- Tziperman, E., and B. F. Farrell (2009), Pliocene equatorial temperature: Lessons from atmospheric superrotation, *Paleoceanography*, *24*, PA1101, doi:10.1029/2008PA001652.
- Wara, M. W., A. C. Ravelo, and M. L. Delaney (2005), Permanent El Niño-like conditions during the Pliocene warm period, *Science*, *309*, 758–761.
- Winant, C. D., and C. E. Dorman (1997), Seasonal patterns of surface wind stress and heat flux over the Southern California Bight, *J. Geophys. Res.*, *102*(C3), 5641–5653.
- Woodard, S. C., Y. Rosenthal, K. G. Miller, J. D. Wright, B. K. Chiu, and K. T. Lawrence (2014), Antarctic role in Northern Hemisphere glaciation, *Science*, *346*(6211), 847–851.
- Zhang, Y. G., M. Pagani, and Z. Liu (2014), A 12-million-year temperature history of the tropical Pacific Ocean, *Science*, *344*(6179), 84–87.